J Mater Sci (2017) 52:305–313

Wear resistance and electroconductivity in a Cu–0.3Cr–0.5Zr alloy processed by ECAP

A. P. Zhilyaev[1,2,3,*], A. Morozova[4], J. M. Cabrera[5], R. Kaibyshev[4], and T. G. Langdon[6]

[1] Institute for Metals Superplasticity Problems, Khalturina 39, Ufa, Russia 450001
[2] Fundació CTM Centre Tecnològic, Plaça de la Ciencia 2, Manresa, 08242 Barcelona, Spain
[3] Research Laboratory for Mechanics of New Nanomaterials, St. Petersburg State Polytechnical University, Polytechnicheskaya 29 St., Petersburg, Russia 195251
[4] Belgorod State University, Pobeda 85, Belgorod, Russia 308015
[5] Departamento de Ciencia de los Materiales e Ingeniería Metalúrgica, ETSEIB–Universitat Politècnica de Catalunya, Av. Diagonal 647, 08028 Bacelona, Spain
[6] Materials Research Group, Faculty of Engineering and the Environment, University of Southampton, Southampton SO17 1BJ, UK

Received: 2 August 2016
Accepted: 22 August 2016
Published online: 30 August 2016

ABSTRACT

The ultrafine-grained microstructures and functional properties, including wear resistance for dry sliding and electrical conductivity, were investigated in a Cu–0.3 %Cr–0.5 %Zr alloy processed by equal-channel angular pressing (ECAP) at a temperature of 400 °C to total strains of 1, 2, and 4. Severe plastic deformation by ECAP to a total strain of ~1 led to a significant decrease in the wear resistance because of the rapid surface damage to both solution-treated (ST) and aged (AT) samples where a high density of dislocations was arranged in stochastic low-angle subboundaries by brittle fracture. Further deformation by subsequent ECAP passes promoted the subdivision of the shear bands by geometrically necessary boundaries. Correspondingly, the number of fine crystallites outlined by high-angle boundaries increased, and the wear rate decreased. After four ECAP passes, the wear rate decreased to the level of the initial state of the alloy and equaled 1.68×10^{-5} mm^3/(N m) and 1.40×10^{-5} mm^3/(N m) for ST and AT samples, respectively. The results demonstrate that the damage mechanism is the controlling factor for wear resistance of Cu–Cr–Zr bronze hardened by intense plastic straining.

Introduction

A combination of grain refinement and precipitation hardening is a well-established procedure for improving mechanical and functional properties such as yield strength and wear resistance. Currently, the design of highly conductive materials for fusion, high-speed railroad, or generation IV reactors is of major importance in order to accomplish industrial requirements [1–3]. For example, there is a demand to

Address correspondence to E-mail: AlexZ@anrb.ru

DOI 10.1007/s10853-016-0331-8

improve the strength and conductivity performance of the contact wires in the electric connections of high-speed trains [4–6]. In practice, the target for the new material of the contact wires is an alloy having a tensile strength greater than 530 MPa and an electrical conductivity of over 78 pct of the International Annealed Copper Standard (IACS). In addition, a high wear resistance is a critical issue. According to the commonly used relationship [7, 8] the wear rate is the reciprocal of the hardness of the contact materials:

$$Q = K \cdot F \cdot L/H_V, \quad (1)$$

where Q is the total volume of the wear debris produced, K is a dimensionless constant, F is the total normal load, L is the sliding distance, and H_V is the hardness of the softest contacting surfaces. The wear rate, W, follows from Eq. (1) as

$$W = Q/(F \cdot L) = K/H_V \quad (2)$$

In order to accomplish the above specifications, the Cu–Cr–Zr alloy is considered as one of the best candidates for industrial applications. Thus, this alloy can be subjected to thermo-mechanical processes to achieve the desired properties. Recently, some approaches were developed for strengthening commercially pure copper [9, 10] and Cu–Cr–Zr alloys, while retaining their electric conductivity at a sufficiently high level of 80 % IACS [11–19]. These processes involve the introduction of intense plastic deformation at an elevated temperature, thereby enabling a good combination of strength and electroconductivity [20, 21]. However, it is important to note that the wear properties have not yet been investigated.

Accordingly, this report focusses on the wear resistance of the Cu–0.3Cr–0.5Zr alloy subjected to equal-channel angular pressing (ECAP). Particular attention is paid to the significance of the near-surface microstructure in the wear process [22]. As was shown earlier for copper [23], there is no unambiguous relation between the hardness of the contact material and the wear rate.

Experimental material and procedures

An alloy of Cu–0.35Cr–0.5Zr (wt%) subjected to two treatments (solution treated (ST) and age hardened (AT)) was processed by ECAP under an isothermal condition at 400 °C to total strains of ~1, 2, and 4. The billets with starting dimensions of $14 \times 14 \times 90$ mm^3 were preheated for 30 min and then pressed through a die having an internal angle of 90° which leads to a strain of ~1 on each pass through the die [24]. Repetitive passes were conducted using processing route B_C in which each billet is rotated by 90° in the same sense between each pass [25]. The processed samples were cooled in water after reaching the required total strain. Full details on the sample preparation for microstructural investigations can be found elsewhere [21].

The electrical conductivities of the investigated samples were measured using the four-point probe method. The wear resistance of the samples was estimated using a high-temperature CSM tribometer oscillating friction and wear tester with a ball-on-disk contact configuration. The surfaces of the investigated samples were mechanically polished using a diamond suspension with a final particle size of 3 μm. The sliding tests were carried out at ambient temperature with a load of 1.5 N, a sliding speed of 0.04 m/s, and a sliding distance of 100 m using ∅6 mm steel balls. After completing the wear tests, a precision contact profilometer from SURTRONIC was used to acquire the profiles of the wear tracks at selected points on the specimens.

Results and discussion

Table 1 summarizes all the experimental data acquired in this investigation. The mean friction coefficient and the Kernel average misorientation (KAM) decrease with increasing numbers of ECAP passes for both ST and AT treatments. The wear rate demonstrates a nonmonotonic behavior for both ST and AT treatments, increasing for the samples processed by one pass and then decreasing almost to the initial value with increasing numbers of ECAP passes. The Taylor factor possesses a stability of approximately 3.2 ± 0.1 for the ST specimen and 3.3 ± 0.1 for the AT specimen of the Cu–Cr–Zr alloy. The electroconductivity decreases with increasing accumulated strain and stabilizes at a level of 2.0×10^7 $(\Omega\ m)^{-1}$ which is 34.5 % of the electroconductivity for the IACS. The mean grain (sub-grain) size decreases and the dislocation density increases with increasing numbers of ECAP passes.

Figure 1 depicts the EBSD maps (first and second columns) and the SEM micrographs of wear tracks of

Table 1 Experimental data

Number of ECAP passes	Mean friction coefficient		Wear rate, $\times 10^{-5}$ (mm^3/N m)		KAM (°)		Taylor factor		Electroconductivity*, $\times 10^7$ $(\Omega\ m)^{-1}$		(Sub) grain size (nm)		Dislocation density, $\times 10^{14}$ (m^{-2})	
	ST	AT	ST	AT	ST	AT	ST	AT	ST	AT	ST	AT	ST	AT
0	0.80	0.80	1.79	1.30	1.75	1.75	3.30	3.30	2.00	2.84	>1000	>1000	0.1	0.1
1	0.70	0.72	7.86	7.09	1.28	0.93	3.12	3.34	1.53	2.00	420	570	8.3	7.3
2	0.65	0.70	2.77	2.82	0.91	0.92	3.14	3.38	1.66	2.00	340	350	13.0	13.4
4	0.62	0.66	1.68	1.40	0.91	0.80	3.20	3.26	1.81	2.00	330	340	14.0	12.6

* IACS $= 5.8 \times 10^7\ (\Omega\ m)^{-1}$

the solution-treated Cu–Cr–Zr alloy for different numbers of ECAP passes from the initial condition to 4 passes. The EBSD maps consist of a kernel average misorientation (KAM) map and a map of the Taylor factor. Correspondingly, Fig. 2 shows the same types of maps and SEM micrographs for the aged Cu–Cr–Zr alloy. The black lines in the EBSD maps separate grains with high-angle boundaries (HABs). The EBSD maps for samples subjected to both treatments appear to be rather similar with some shear bands revealed in the microstructures. Some typical shear bands with a mean width of ~2–5 μm are marked by light dashed lines (yellow in the online version). Commonly, the density of HAB and the number of the fine highly misoriented crystallites, especially those located within the shear bands, increase during ECAP. The wear tracks in the right columns of Figs. 1 and 2 possess some specific strands that apparently correlate with the shear bands highlighted in the EBSD maps. Moreover, the worn surfaces of the ST and AT specimens evolve in a similar way for the initial specimen and the ECAP samples processed by 1, 2, and 4 passes. No significant amount of debris was found on the wear tracks of the initial specimens (Figs. 1, 2). On the contrary, the SEM micrographs for the specimens processed by one ECAP pass demonstrate heavily damaged surfaces which occupy nearly the whole area of the micrographs for both the ST and AT samples. The fracture surfaces are of a significantly brittle appearance. The specimens subjected to 2 and 4 passes of ECAP possess moderately damaged areas with noticeably decreased areas of worn strands (Figs. 1, 2). It is also apparent that after four ECAP passes, the AT specimen undergoes a transition from brittle to ductile behavior whereas the ST specimen retains the brittle fracture surface. The appearance of the worn surfaces is in good correlation with the measured wear rates recorded in Table 1.

The friction coefficient (upper row) and the friction force (lower row) are shown in Fig. 3 for the ECAP AT and ST samples as a function of the sliding distance. The friction coefficients of all ST specimens apparently saturate at a level of ~0.60–0.65, although the friction coefficients of the AT samples saturate at a level of ~0.70–0.75. The friction forces have a tendency to saturate at a level on the order of ~0.9 N for the ST specimens and at a level of ~1.1 N for the AT samples after a sliding distance of approximately 30 m.

Figure 4 shows the experimental parameters, including the mean friction coefficient, wear rate, electroconductivity and Vickers microhardness, and derivatives of some parameters in terms of the rate of dislocation accumulation and rate of microhardness change for the ST and AT Cu–Cr–Zr alloy samples as a function of the number of ECAP passes or the accumulated strain. The upper row of Fig. 4 depicts the mean friction coefficients (Fig. 4a) and the wear rates (Fig. 4b) for the ST and AT Cu–Cr–Zr alloy samples as a function of the number of ECAP passes. There is a clear trend showing a decrease in the mean friction coefficient with an increase in the accumulated strain for both ST and AT samples. The wear rate possesses a maximum value for samples processed for one ECAP pass. This correlates well with the heavily worn surfaces shown in Figs. 1 and 2 (second row). The second row of Fig. 4 (c, d) shows the change in electroconductivity as a function of the accumulated strain (Fig. 4c) and the rate of dislocation accumulation calculated on the basis of the data in Table 1 (Fig. 4d). As expected, there is a significant

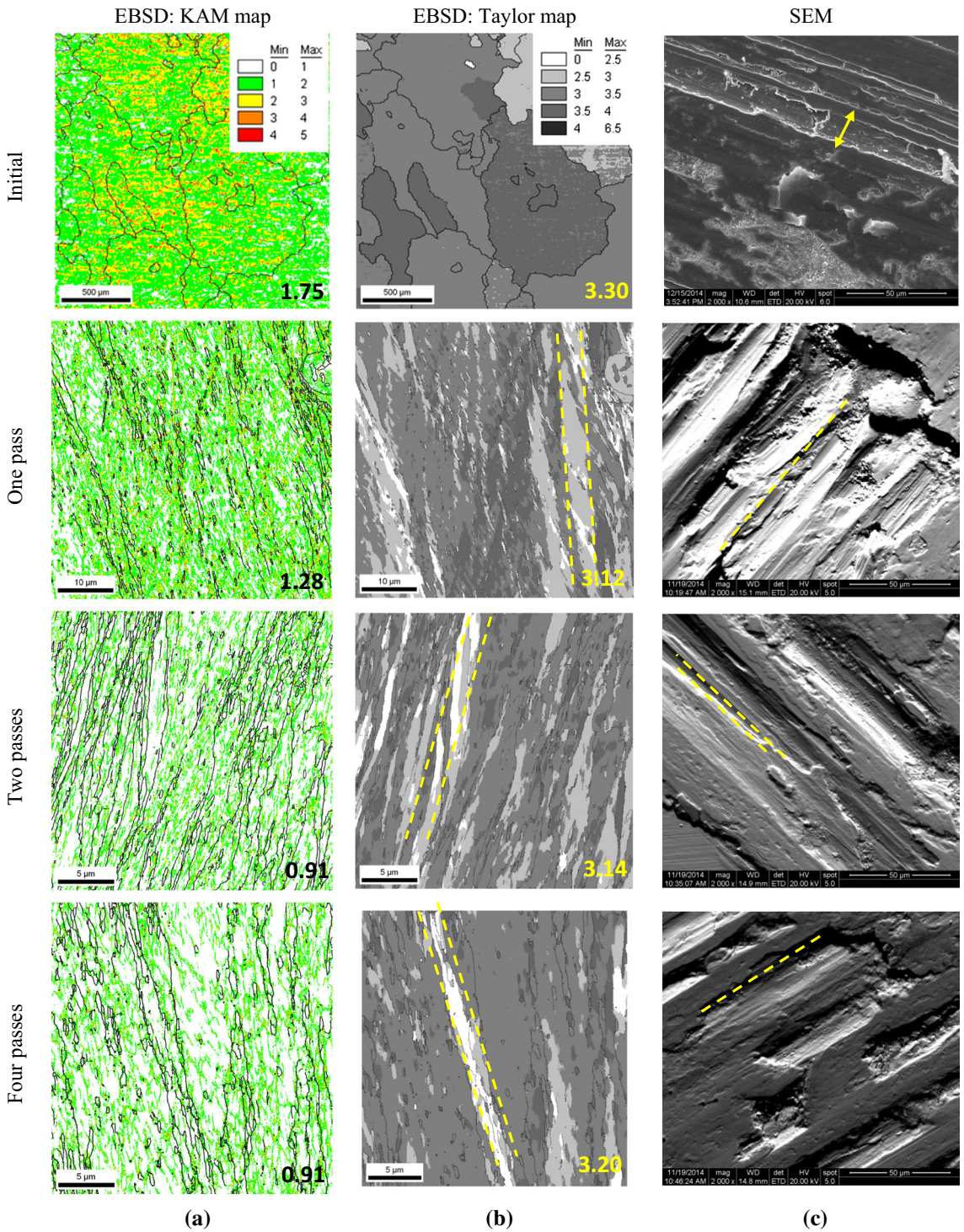

Figure 1 **a** EBSD-KAM map, **b** EBSD-Taylor map, and **c** SEM micrographs of worn surfaces of ECAP Cu–Cr–Zr alloys in solution-treated condition as a function of number of ECAP passes.

drop in conductivity after the alloy is deformed by ECAP for one pass. Additional ECAP straining gives a slight increase in the electroconductivity with increasing numbers of passes. The rate of dislocation accumulation (Fig. 4d) follows the same trend as the wear rate (Fig. 4b). The last row of Fig. 4 shows the microhardness evolution with the number of ECAP passes (Fig. 4e) and its changing rate (Fig. 4f).

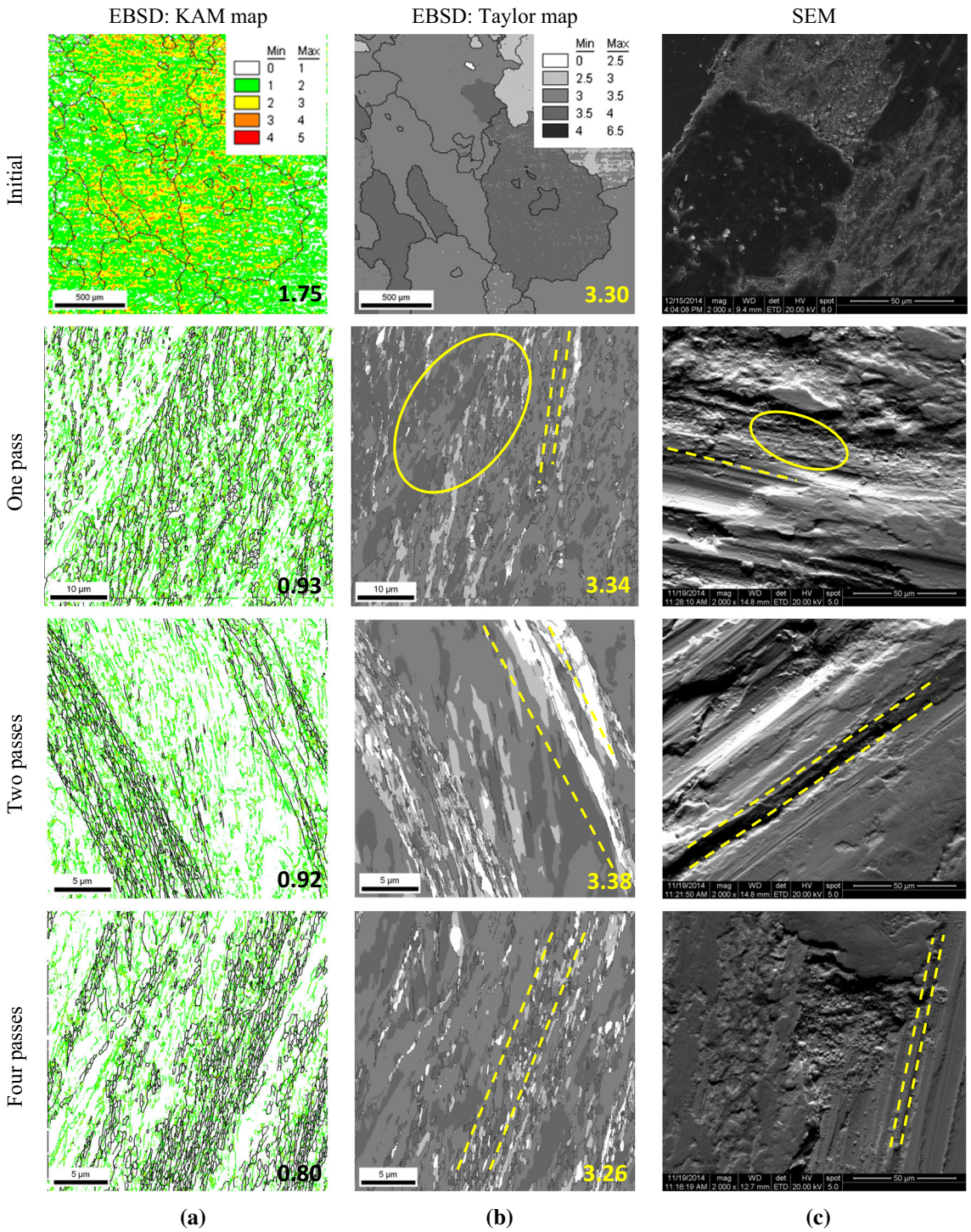

Figure 2 **a** EBSD-KAM map, **b** EBSD-Taylor map, and **c** SEM micrographs of worn surfaces of ECAP Cu–Cr–Zr alloys in aged condition as a function of number of ECAP passes.

From all the dependencies documented in Fig. 4, it may be concluded that the electroconductivity follows an inverse law with microhardness ($\sigma_C \approx 1/Hv$). However, the wear rate does not obey Eq. 1. Apparently, therefore, the wear rate is dictated not by the hardness but rather by the type of damage. The initial material exhibits damage dominated by shear fracture (Fig. 1c) that is attributed to a low material hardness (Fig. 4e). The first pass provides more than a fourfold increase in the

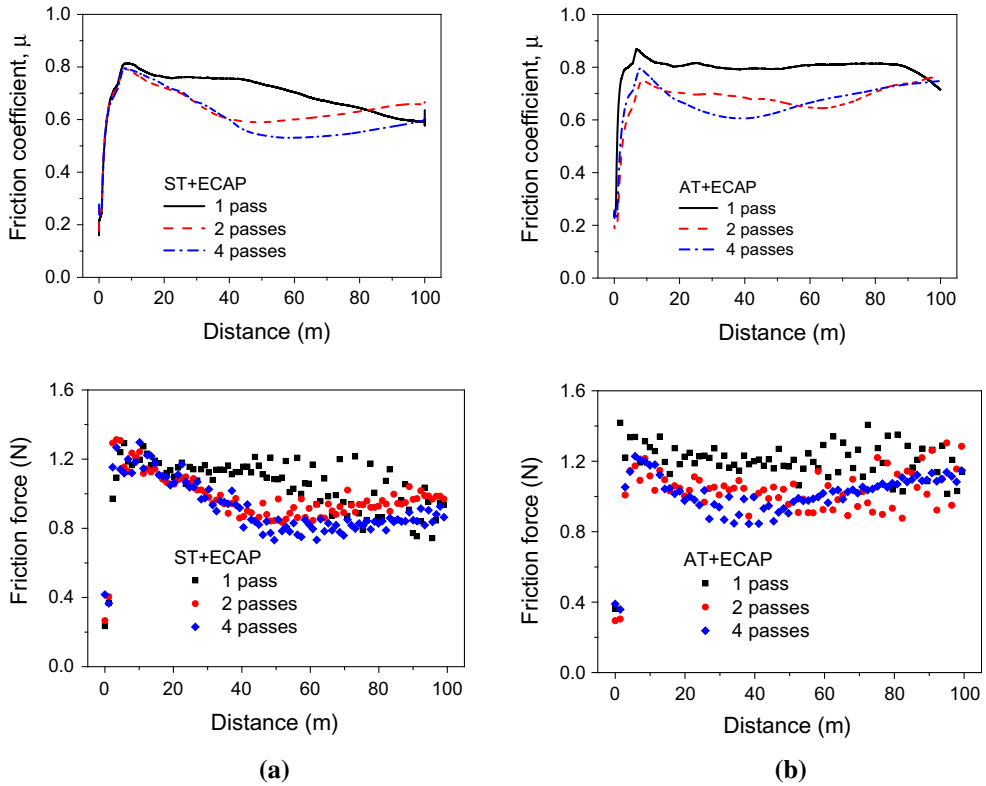

Figure 3 Friction coefficient (*upper row*) and friction force (*lower row*) as a function of the sliding distance for the ECAP Cu–Cr–Zr alloys in **a** solution-treated condition and **b** aged condition.

wear rate of the samples from both treatments (Table 1) despite an increase in hardness. This phenomenon is attributed to the replacement of shear fracture as the dominant damage mechanism by brittle fracture and the subsequent crumbling of relatively large material areas along the shear bands. As straining by ECAP progresses to two passes, the microstructure of the Cu–Cr–Zr alloys alters to thin lamellae separated by high-angle (>15°) or medium-angle (>5°–15°) boundaries. As a result, the brittle fracture damage occurs through the crumbling of relatively thin areas (Fig. 1c). In addition, the dislocation density increases with accumulating strain that leads to an increase in the hardness (Fig. 4e). An approximately threefold decrease in the wear rate takes place (Table 1), and it is evident that the change from crumbling of large areas to the breaking of thin bands strongly contributes to the decreased wear rate. After four ECAP passes, the lamellae were subdivided by transverse boundaries to crystallites of a nearly rectangular shape, and the mixing of thin layers that was responsible for the decrease in the wear rate (Table 1) was rarely observed (Fig. 1c).

It is evident that extended plastic deformation leads to further refining of the microstructure of the Cu–Cr–Zr alloy with moderate and high-angle boundaries, and this decreases the wear rate to the level of the initial state of the alloy. There is no clear difference in the wear properties of the ST and AT samples processed to the same strain by ECAP. By contrast, the wear rate appears to depend sensitively on the character of the dislocation substructure. The shear bands involve a high density of stochastic dislocation subboundaries which are brought out by a moderate ECAP strain (i.e., one ECAP pass), and this leads to a drastic degradation of the wear resistance. However, the dislocation rearrangement leading to the subdivision of the shear bands into new fine grains during subsequent ECAP passes serves to remarkably improve the wear resistance. Therefore, extensive grain refinement is a necessity for the enhancement of the wear resistance of the Cu–Cr–Zr bronze with increased hardness that is attributed to deformation hardening. Conversely, the initial hardening of this material by intense plastic straining may degrade the wear resistance due to the evolution of coarse shear bands.

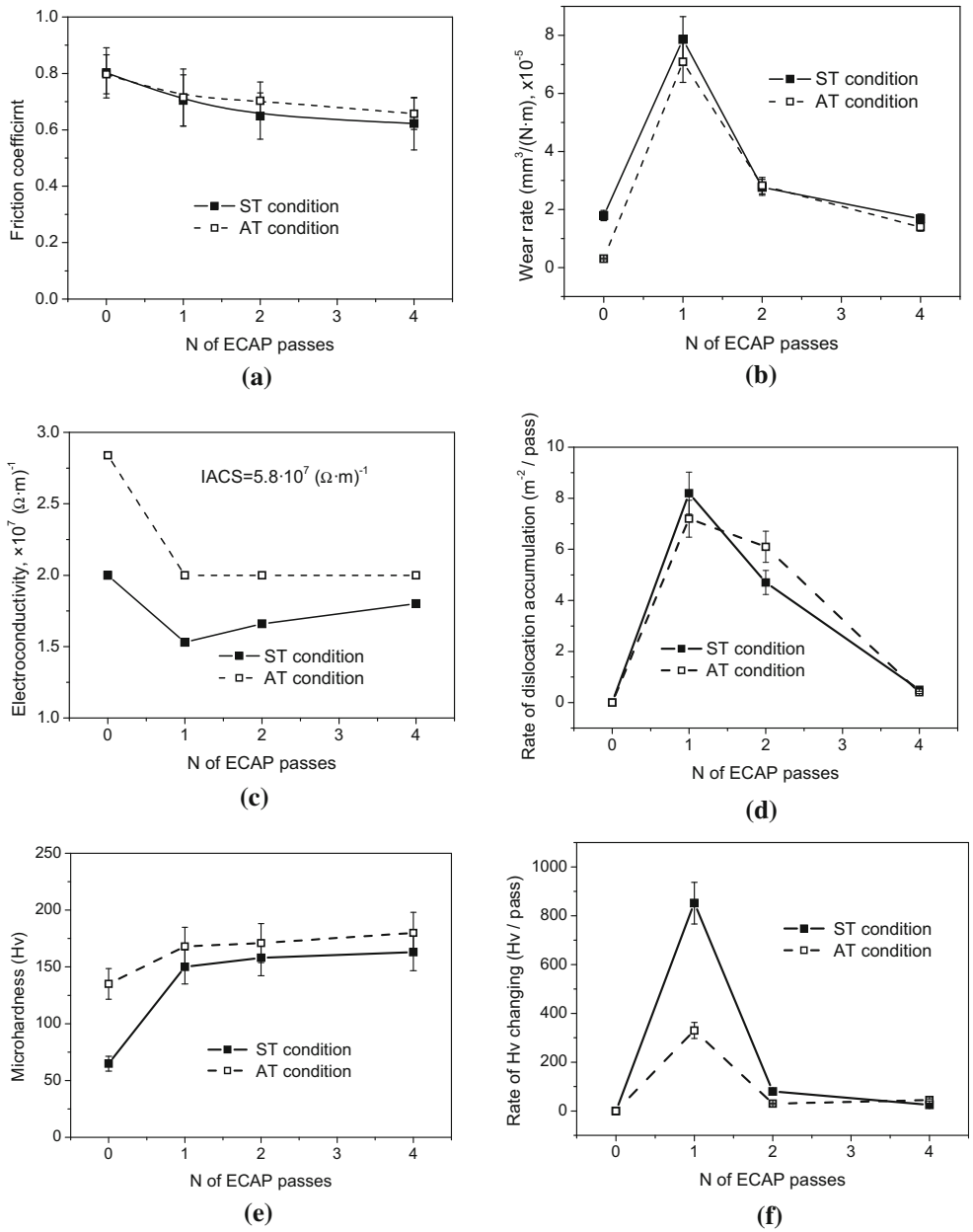

Figure 4 Mean friction coefficient (**a**), wear rate (**b**), electroconductivity (**c**), rate of dislocation accumulation (**d**), Vickers microhardness (**e**) and rate of Hv changing (**f**) for ECAP Cu–Cr–Zr alloys in solution-treated and aged conditions as a function of a number of ECAP passes.

Summary and conclusions

1. Severe plastic deformation by ECAP to a total strain of ~1 leads to a significant decrease in the wear resistance of a Cu–Cr–Zr alloy in dry sliding experiments because of the rapid surface damage introduced in both ST and AT samples where a high density of dislocations was arranged in stochastic low-angle subboundaries by brittle fracture.
2. Further deformation by subsequent ECAP passes promotes the subdivision of the shear bands by geometrically necessary boundaries. Correspondingly, the number of fine crystallites outlined by HABs increases, and the wear rate decreases. After four ECAP passes, the wear rate of dry

sliding decreased to the level of the initial state of the alloy and equaled 1.68×10^{-5} mm^3/(N m) and 1.40×10^{-5} mm^3/(N m) for ST and AT samples, respectively.

3. The damage mechanism is the controlling factor determining the wear resistance of Cu–Cr–Zr bronze hardened by intense plastic straining.

Acknowledgements

AM and RK acknowledge financial support from the Ministry of Science and Education, Russia, under Grant No. 14.Y31.16.8446-NSH and APZ acknowledges a TECNIOSPRING grant financed by Generalitat de Catalunya and co-funded by the 7th Framework program of the EU and the Russian Science Foundation (Project 14-29-00199). TGL acknowledges support from the European Research Council under ERC Grant Agreement No. 267464-SPDMETALS.

Compliance with ethical standards

Conflict of Interest The authors declare that they have no conflict of interest.

References

[1] Topuz AI (2015) Enabling microstructural changes of FCC/BCC alloys in 2D dislocation dynamics. Mater Sci Eng A 627:381–390

[2] Correia JB, Davies HA, Sellars CM (1997) Strengthening in rapidly solidified age hardened Cu–Cr and Cu–Cr–Zr alloys. Acta Mater 45:177–190

[3] ITER Joint Central Team (1994) The impact of materials selection on the design of the International Thermonuclear Experimental Reactor (ITER). J Nucl Mater 212–215:3–10

[4] Liu Q, Zhang X, Ge Y, Wang J, Cui JZ (2006) Effect of processing and heat treatment on behavior of Cu–Cr–Zr alloys to railway contact wire. Metal Mater Trans A 37:3233–3238

[5] Batra IS, Dey GK, Kulkarni UD, Banerjee S (2001) Microstructure and properties of a Cu–Cr–Zr alloy. J Nucl Mater 299:91–100

[6] Ghosh G, Miyake J, Fine ME (1997) The systems-based design of high strength, high-conductivity alloys. JOM 49:56–60

[7] Archard JF (1953) Contact and rubbing of flat surfaces. J Appl Phys 24:981–988

[8] Archard JF, Hirst W (1956) The wear of metals under unlubricated conditions. Proc Royal Soc A 236:397–410

[9] Zhilyaev AP, Gimazov AA, Langdon TG (2013) Recent developments in modelling of microhardness saturation during SPD processing of metals and alloys. J Mater Sci 48:4461–4466. doi:10.1007/s10853-013-7155-6

[10] Zhilyaev AP, Swaminathan S, Pshenichnyuk AI, Langdon TG, McNelley TR (2013) Adiabatic heating and the saturation of grain refinement during SPD of metals and alloys: experimental assessment and computer modelling. J Mater Sci 48:4626–4636. doi:10.1007/s10853-013-7254-4

[11] Belyakov A, Murayama M, Sakai Y, Tsuzaki K, Okubo M, Eto M, Kimura T (2006) Development of a high-strength high-conductivity Cu–N–P alloy. Part II: processing by severe deformation. J Electr Mater 35:2000–2008

[12] Wei KX, Wei W, Wang F, Dua QB, Alexandrov IV, Hu J (2011) Microstructure, mechanical properties and electrical conductivity of industrial Cu–0.5% Cr alloy processed by severe plastic deformation. Mater Sci Eng A 528:1478–1484

[13] Vinogradov A, Patlan V, Suzuki Y, Kitagawa K, Kopylov VI (2002) Structure and properties of ultra-fine grain Cu–Cr–Zr alloy produced by equal-channel angular pressing. Acta Mater 50:1639–1651

[14] Shakhova I, Yanushkevich Z, Fedorova I, Belyakov A, Kaibyshev R (2014) Grain refinement in a Cu–Cr–Zr alloy during multidirectional forging. Mater Sci Eng A 606:380–389

[15] Murashkin MY, Sabirov I, Sauvage X, Valiev RZ (2016) Nanostructured Al and Cu alloys with superior strength and electrical conductivity. J Mater Sci 51:33–49. doi:10.1007/s10853-015-9354-9

[16] Zhilyaev AP, Shakhova I, Belyakov A, Kaibyshev R, Langdon TG (2014) Effect of annealing on wear resistance and electroconductivity of copper processed by high-pressure torsion. J Mater Sci 49:2270–2278. doi:10.1007/s10853-013-7923-3

[17] Shangina D, Maksimenkova Y, Bochvar N, Serebryany V, Raab G, Vinogradov A, Skrotzki W, Dobatkin S (2016) Influence of alloying with hafnium on the microstructure, texture, and properties of Cu–Cr alloy after equal channel angular pressing. J Mater Sci 51:5493–5501. doi:10.1007/s10853-016-9854-2

[18] Chbihi A, Sauvage X, Blavette D (2014) Influence of plastic deformation on the precipitation of Cr in copper. J Mater Sci 49:6240–6247. doi:10.1007/s10853-014-8348-3

[19] Shangina DV, Gubicza J, Dodony E, Bochvar NR, Straumal PB, Tabachkova NY, Dobatkin SV (2014) Improvement of strength and conductivity in Cu-alloys with the application of high pressure torsion and subsequent heat-treatments. J Mater Sci 49:6674–6681. doi:10.1007/s10853-014-8339-4

[20] Mishnev R, Shakhova I, Belyakov A, Kaibyshev R (2015) Deformation microstructures, strengthening mechanisms, and electrical conductivity in a Cu–Cr–Zr alloy. Mater Sci Eng A 629:29–40

[21] Zhilyaev AP, Shakhova I, Morozova A, Belyakov A, Kaibyshev R (2016) Grain refinement kinetics and strengthening mechanisms in Cu–0.3Cr–0.5Zr alloy subjected to intense plastic deformation. Mater Sci Eng A 654:131–142

[22] Rigney DA, Glaeser WA (1978) The significance of near surface microstructure in the wear process. Wear 45:241–250

[23] Zhilyaev AP, Shakhova I, Belyakov A, Kaibyshev R, Langdon TG (2013) Wear resistance and electroconductivity in copper processed by severe plastic deformation. Wear 305:89–99

[24] Iwahashi Y, Wang J, Horita Z, Nemoto M, Langdon TG (1996) Principle of equal-channel angular pressing for the processing of ultrafine-grained materials. Scripta Mater 35:143–146

[25] Furukawa M, Iwahashi Y, Horita Z, Nemoto M, Langdon TG (1998) The shearing characteristics associated with equal-channel angular pressing. Mater Sci Eng A 257:328–332